applied optics

Efficient generation of Hermite–Gauss and Ince–Gauss beams through kinoform phase elements

Dilia Aguirre-Olivas,* Gabriel Mellado-Villaseñor, David Sánchez-de-la-Llave, and Victor Arrizón

Instituto Nacional de Astrofísica, Óptica y Electrónica, Luis Enrique Erro #1, 72840 Tonantzintla, Puebla, Mexico
**Corresponding author: dilia_aguirre@inaoep.mx*

Received 17 July 2015; revised 3 September 2015; accepted 3 September 2015; posted 3 September 2015 (Doc. ID 246290); published 30 September 2015

We discuss the generation of Hermite–Gauss and Ince–Gauss beams employing phase elements whose transmittances coincide with the phase modulations of such beams. A scaled version of the desired field appears, distorted by marginal optical noise, at the element's Fourier domain. The motivation to perform this study is that, in the context of the proposed approach, the desired beams are generated with the maximum possible efficiency. A disadvantage of the method is the distortion of the desired beams by the influence of several nondesired beam modes generated by the phase elements. We evaluate such distortion employing the root mean square deviation as a figure of merit.

OCIS codes: (050.1940) Diffraction; (350.7420) Waves; (090.1760) Computer holography; (230.6120) Spatial light modulators.

http://dx.doi.org/10.1364/AO.54.008444

1. INTRODUCTION

It is well known that Hermite–Gauss (HG) and Ince–Gauss (IG) beams are solutions of the paraxial wave equation in Cartesian and elliptic cylindrical coordinates, respectively [1,2]. Each one of these sets of fields forms a complete orthogonal basis under which any function can be represented. These fields, together with the Laguerre–Gauss beams, which are solutions of the paraxial wave equation in circular cylindrical coordinates, belong to the class of structurally stable optical fields. Consequently, they are also self-transforming fields under the Fourier transform operation. In the past, we have shown that the efficient generation of certain fields that are invariant under propagation can be realized using kinoform phase elements (KPEs) [3–5]. The KPE of a complex optical field has a phase transmittance that coincides with the phase modulation of such a field. Recently, this codification technique was employed in the generation of Mathieu–Gauss beams [6] and Laguerre–Gauss beams [7]. A phase diffractive optical element (DOE) for generating IG beams has been previously reported [8]. The phase of this DOE is given by the phase of the desired IG beam, attenuated by the beam amplitude. In this work, we propose to employ KPEs to synthesize the structurally stable HG and IG beams. The Fourier transform of the desired beam, which is a scaled version of it, is generated at the KPE Fourier domain with relatively low noise. In Section 2, we review the mathematical description of the HG and IG beams. Using the orthonormal series of these beams, we analyze theoretically its efficient generation using the kinoform technique. In Section 3, we define the accuracy and efficiency parameters for evaluating the KPE performance. A crucial feature of a KPE is the size of its bounding pupil, which is subjected to an optimization process that minimizes the RMS error of the generated beam with respect to the desired beam. The numerically computed values of efficiency and RMS are reported in Section 3, for a variety of cases. Experimental results that corroborate our proposal are presented in Section 4. In Section 5, we explain why the Fourier transform of the desired HG and IG beams appears, with relatively low error, at the KPE Fourier plane. At the end of Section 5, we present final remarks and conclusions.

2. HERMITE–GAUSS AND INCE–GAUSS KINOFORMS

The HG beams are exact solutions of the scalar paraxial wave equation in Cartesian coordinates. Their complex amplitude is expressed, at the waist plane $z = 0$, as

$$f_{p,q}(x, y; w_o) = H_p\left(\frac{\sqrt{2}}{\omega_o}x\right) H_q\left(\frac{\sqrt{2}}{\omega_o}y\right) \exp\left(-\frac{r^2}{w_o^2}\right), \quad (1)$$

where H_l $(l = p, q)$ is the lth-order Hermite polynomial, ω_o is the beam waist, and $r = (x^2 + y^2)^{1/2}$ is the transverse radial coordinate. Let us assume that the HG beam that we desire

to generate is $f_{m,n}(x,y;w_o)$. The proposed KPE of this beam is given by

$$k_{m,n}(x,y;w_o)=\text{sign}[f_{m,n}(x,y;w_o)]\text{rect}\left(\frac{x}{a}\right)\text{rect}\left(\frac{y}{b}\right), \quad (2)$$

where sign(σ) is equal to 1 for $\sigma \geq 0$ and −1 otherwise, while the product of the unidimensional rect functions represent a rectangular pupil of sides a and b. The presence of the rectangular pupil that limits the KPE transmittance in Eq. (2) is crucial. The dimensions of this pupil have critical values that are obtained employing an iterative optimization process, which is described below.

Since the HG functions defined in Eq. (1) form a complete orthogonal basis in $\mathbb{R}^2$, the KPE transmittance in Eq. (2) is given by the series

$$k_{m,n}(x,y;w_o)=\sum_{p=0}^{\infty}\sum_{q=0}^{\infty}A_{p,q}f_{p,q}(x,y;w_o), \quad (3)$$

with coefficients

$$A_{p,q}=\iint_{-\infty}^{\infty}k_{m,n}(x,y;w_o)\frac{f_{p,q}(x,y;w_o)}{h_{p,q}}\text{d}x\text{d}y, \quad (4)$$

and $h_{p,q}=2^{p+q}p!q!\pi\omega_o^2/2$. It is noteworthy that the term with indices $p=m$ and $q=n$, in Eq. (3), corresponds to the desired HG beam $f_{m,n}(x,y;w_o)$, with a weighting factor $A_{m,n}$. In general, the argument of the integral in Eq. (4) presents many sign oscillations that tend to reduce the absolute value of the coefficients $A_{p,q}$. However, the integral argument for the coefficient $A_{m,n}$ (and only for this coefficient) is a non-negative function. In consequence, the (m,n)-order term in Eq. (3), which corresponds to the desired field, tends to be dominant. Indeed, it can be shown that the KPE of the desired HG field is the phase DOE whose expansion in orthogonal modes contains this field with the maximum possible weighting factor. In order to prove this result, let us consider a generic phase DOE with transmittance

$$h(x,y)=\exp[i\psi(x,y)]\text{rect}\left(\frac{x}{a}\right)\text{rect}\left(\frac{y}{b}\right), \quad (5)$$

which possess an arbitrary phase $\psi(x,y)$, within the domain that corresponds to the rectangular pupil $\text{rect}(x/a)\text{rect}(y/b)$.

We can relate the DOE transmittance $h(x,y)$ with the transmittance of the desired field $f_{m,n}(x,y;w_o)$. This can be done by representing the function $h(x,y)$ in Eq. (5) by its orthogonal series in the basis of HG modes defined in Eq. (1), obtaining

$$h(x,y)=B_{m,n}f_{m,n}(x,y;w_o)+d_{m,n}(x,y;w_o), \quad (6)$$

where

$$d_{m,n}(x,y;w_o)=\sum_{(p,q)\neq(m,n)}^{\infty}B_{p,q}f_{p,q}(x,y;w_o), \quad (7)$$

and coefficients $B_{p,q}$ are computed by the integral in Eq. (4) replacing the function $k_{m,n}(x,y,wo)$ by $h(x,y)$. It is interesting to note that the desired mode $f_{m,n}(x,y;w_o)$ and the term $d_{m,n}(x,y;w_o)$, in Eq. (6), are mutually orthogonal, i.e., their internal product is null. Thus, expressing the desired mode as $f_{m,n}(x,y,w_o)=a(x,y)\exp[i\phi(x,y)]$ and performing the internal product with $f_{m,n}(x,y,w_o)$ on both sides of Eq. (6), we obtain

$$|B_{m,n}|=C\left|\iint_{\Omega}a(x,y)\exp\{i[\psi(x,y)-\phi(x,y)]\}\text{d}x\text{d}y\right|, \quad (8)$$

where $C=(\iint_{\Omega}a^2(x,y)\text{d}x\text{d}y)^{-1}$ and the integration domain Ω corresponds to the pupil that limits the transmittance $h(x,y)$. In Eq. (8) we note that the upper bound limit for $|B_{m,n}|$, given by $C|\iint_{\Omega}a(x,y)\text{d}x\text{d}y)|$, is obtained when

$$\exp[i\psi(x,y)]=\exp[i\phi(x,y)], \quad (9)$$

i.e., when the phase of the DOE is identical to the phase of the desired field $f_{m,n}(x,y;w_o)$ [9]. According to this result, the orthogonal series of the phase DOE, whose transmittance coincides with the phase modulation of the desired HG beam, contains this beam with the maximum possible weighting factor. On the other hand, from Eq. (6) we note that the DOE efficiency, in the generation of the desired field, is proportional to $|B_{m,n}|^2$. Thus, the upper bound limit for $|B_{m,n}|$ also ensures a maximum value for the DOE efficiency.

Other fields to be synthesized are the even and odd IG beams. They are solutions of the scalar paraxial wave equation in elliptical coordinates and are written, at the waist plane $z=0$, as

$$f_{p,q}^{e}(\xi,\chi;w_o)=C_{p,q}(i\xi)C_{p,q}(\chi)\exp\left(-\frac{r^2}{\omega_o^2}\right), \quad (10a)$$

$$f_{p,q}^{o}(\xi,\chi;w_o)=S_{p,q}(i\xi)S_{p,q}(\chi)\exp\left(-\frac{r^2}{\omega_o^2}\right), \quad (10b)$$

where $C_{p,q}$ and $S_{p,q}$ are, respectively, the even and odd Ince polynomials of order p and degree q. The integer indices p and q, which are in the ranges of $0\leq q\leq p$ and $1\leq q\leq p$ for even and odd functions, respectively, always have the same parity, i.e., $(-1)^{p-q}=1$. The variables χ and ξ are the radial and angular elliptic coordinates defined by $x=\omega_o(\epsilon/2)^{1/2}\cosh\xi\cos\chi$ and $y=\omega_o(\epsilon/2)^{1/2}\sinh\xi\sin\chi$, where ϵ is the ellipticity parameter. The transmittance of the KPE proposed to generate the beam $f_{m,n}^{\alpha}(\xi,\chi;w_o)$ is given by

$$k_{m,n}^{\alpha}(\xi,\chi;w_o)=\text{sign}[f_{m,n}^{\alpha}(\xi,\chi;w_o)]P(x,y), \quad (11)$$

where $\alpha=\{e,o\}$ and $P(x,y)$ is an elliptical pupil, equal to 1 for $(\frac{x^2}{a^2}+\frac{y^2}{b^2})\leq 1$ and 0 otherwise. Similar to the rectangular pupil for HG beams, the dimensions of the elliptical aperture for IG beams are also subjected to an optimization process.

Since each set of IG beams in Eqs. (10a) and (10b) represents an orthonormal complete basis in $\mathbb{R}^2$ [10], the KPE in Eq. (11) can be expressed by the series

$$k_{m,n}^{\alpha}(\xi,\chi;w_o)=\sum_{p=0}^{\infty}\sum_{q=0}^{p}A_{p,q}^{\alpha}f_{p,q}^{\alpha}(\xi,\chi;w_o), \quad (12)$$

with coefficients

$$A_{p,q}^{\alpha}=\iint_{-\infty}^{\infty}k_{m,n}^{\alpha}(\xi,\chi;w_o)f_{p,q}^{\alpha}(\xi,\chi;w_o)\text{d}S. \quad (13)$$

It is noteworthy that the (m,n)th term of the series in Eq. (12) corresponds to the encoded beam $f_{m,n}^{\alpha}(\xi,\chi;w_o)$, with a weighting factor $A_{m,n}^{\alpha}$. It is also noteworthy that the integrand in

Eq. (13), expressed for $A^{\alpha}_{m,n}$, becomes non-negative and maximizes the modulus of this coefficient. Similar to the case of KPEs for HG beams, it can be shown that the orthogonal series of the KPE for the desired IG beam contains this field with the maximum possible weighting factor.

In principle, the above results point toward a convenient generation of the desired HG and IG fields using their KPE s. In Section 3 we will optimize and evaluate the HG and IG beams generated at the Fourier domain of their KPEs.

3. ACCURACY OPTIMIZATION AND EFFICIENCY

In this section, we present an initial performance evaluation of KPEs as generators of HG and IG beams. A complementary evaluation is presented in Section 4. First we focus our attention on the KPE pupil size. This size is critical for the efficient generation of the desired field. We look for the pupil size that minimizes the RMS deviation of the generated beam, with respect to the desired beam.

Since the KPEs in Eqs. (2) and (11) present uniform intensity, within their limiting pupils, the desired HG and IG beams are not visible at the planes of these phase elements. However, it is found that scaled versions of these beams, given by their Fourier transforms, are clearly distinguished at the Fourier domains of the KPEs. An analytic and qualitative explanation of this result is discussed in Section 5. For the moment, we present an initial assessment of the beams generated by the KPEs, in the context of the pupils' optimization.

We start the optimization of the limiting pupil, for any of the KPEs, by determining the initial pupil dimensions a_o and b_o. To illustrate the determination of these dimensions we consider the HG beam $f_{4,4}(x, y; w_o)$, whose modulus and phase are displayed in Fig. 1. In Fig. 1(a) we show horizontal and vertical reference lines (dotted trace) that cross the peak amplitude points at the corners of the field. The initial pupil, depicted in dashed lines, is determined by the points in the reference lines where the amplitude field is 1/100 of the adjacent peak amplitude. Two of these points, at the top of the image, are identified by arrows. The initial pupil dimensions of the KPE are optimized in order to obtain the desired field, at the Fourier domain of this phase DOE, with the minimum RMS. For an arbitrary function $f(x, y)$, expressed in rectangular coordinates (x, y), we employ the following definition for its 2D Fourier transform:

$$F(u, v) = \int_{-\infty}^{\infty} \int_{-\infty} f(x, y) \exp[-i2\pi(ux + vy)]\mathrm{d}x\mathrm{d}y. \quad (14)$$

Using this definition, we compute the Fourier transforms ($\mathfrak{F}$) of the desired fields as $F_{m,n}(u, v; w_o) = \mathfrak{F}\{f_{m,n}(x, y; w_o)\}$ and $F^{\alpha}_{p,q}(u, v; w_o) = \mathfrak{F}\{f^{\alpha}_{p,q}(x, y; w_o)\}$ and for their kinoforms $K_{m,n}(u, v; w_o) = \mathfrak{F}\{k_{m,n}(x, y; w_o)\}$ and $K^{\alpha}_{p,q}(u, v; w_o) = \mathfrak{F}\{k^{\alpha}_{p,q}(x, y; w_o)\}$. The quality of the approximated version of the desired HG beam, obtained at the Fourier domain of the KPE, is evaluated by means of the RMS deviation

$$\mathrm{RMS} = \left[S^{-1} \int_D |F_{m,n} - \gamma \cdot K_{m,n}|^2 \mathrm{d}S\right]^{1/2}, \quad (15)$$

where D is the integration domain, with area S, and γ is a constant that allows the best fitting between the field $F_{m,n}$ and the field $K_{m,n}$ produced by the kinoform. The integration domain D is a rectangular pupil that is established with the same criterion that the initial pupil in the KPE plane, i.e., the decay of the desired field is 1/100 of its peak value at the edges of the domain D. In Eq. (15), the beams $F_{m,n}$ and $K_{m,n}$ are, respectively, replaced by $F^{\alpha}_{p,q}$ and $K^{\alpha}_{p,q}$ when the desired field is the IG beam, and the domain D is replaced by an elliptical pupil.

In the third paragraph of this section we described the method to establish the initial KPE pupil dimensions (a_o and b_o). In this process we found four reference lines (dotted trace in Fig. 1) whose intersections define an additional rectangular area (of dimensions a'_o and b'_o), which is inside the field domain. In the considered cases we have found that the optimum KPE pupil dimensions are in the ranges $[a'_o, a_o]$ (horizontal) and $[b'_o, b_o]$ (vertical). Therefore, the optimal pupil dimensions are obtained in the rectangular domain that have two corners at the points $[a'_o, b'_o]$ and $[a_o, b_o]$ (Fig. 2). The trial pupil dimensions are assigned as the points (a_i, b_j) that form a lattice, with lateral resolution δ_x, in this rectangular set. The lattice resolution δ_x is adopted as the pitch length of the employed SLM which is equal to 8 μm. The optimal KPE dimensions are given by the trial pupil dimensions that provide the minimum RMS value.

In the example of Fig. 1, the small and large initial pupils [of dimensions (a'_o, b'_o) and (a_o, b_o), respectively] correspond to the squares formed with dotted and dashed traces, respectively, while the optimized pupil is drawn with a solid trace. A feature of this simple algorithm is that the number of trial points to be tested is relatively small. For example, in the case of the HG

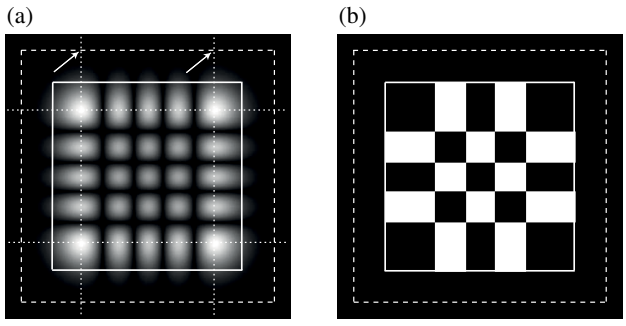

Fig. 1. (a) Modulus and (b) phase of the HG beam $f_{4,4}$. The initial and optimized pupils for the KPE are depicted in dashed trace and solid trace, respectively.

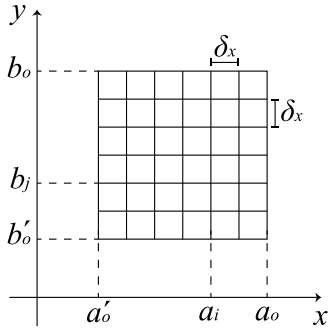

Fig. 2. Rectangular domain for the searching of optimal pupil dimensions. The trial points (a_i, b_j) form a lattice, with lateral resolution δx.

Table 1. RMS for Different HG Beams Generated with Their KPEs

				n			
m	**0**	**1**	**2**	**3**	**4**	**5**	**6**
0	0.0161	0.0183	0.0261	0.0329	0.0345	0.0388	0.0425
1		0.0213	0.0289	0.0363	0.0378	0.0425	0.0463
2			0.0346	0.0403	0.0416	0.0454	0.0487
3				0.0449	0.0455	0.0487	0.0514
4					0.0462	0.0490	0.0515
5						0.0514	0.0535
6							0.0552

beam in Fig. 1, for a waist $w_o = 512$ μm, the number of required trial points was 64×64.

In Table 1 we show the RMS values for several KPEs of HG beams, with optimized pupils. We observe that the RMS increases if any of the beam indices increases, while the other index is fixed. All RMS values, for the considered cases, are smaller than 0.06. We do not include the RMS values below the diagonal in this table because $f_{m,n}$ is a rotated version of $f_{n,m}$. Table 2 shows the values of the optimized RMS for several KPEs of even [part (a)] and odd [part (b)] IG beams. In this case, when $m = n$ the RMS increases with the beam order, and the RMS values are smaller than 0.0935.

The orthogonal series for the KPE [Eq. (3)], which corresponds to the HG mode $f_{m,n}$, contains the HG modes $f_{p,q}$ with weighting factor $A_{p,q}$. Thus, the KPE efficiency in the generation of the HG mode $f_{p,q}$ is given by

$$\eta_{p,q} = \frac{|A_{p,q}|^2 \iint_{-\infty}^{\infty} |f_{p,q}|^2 \mathrm{d}S}{\iint_{-\infty}^{\infty} |k_{m,n}|^2 \mathrm{d}S}. \tag{16}$$

The efficiencies that correspond to the KPEs of IG modes, denoted as $\eta^{\alpha}_{p,q}$ are obtained replacing [in Eq. (16)] $A_{p,q}$, $f_{p,q}$, and $k_{m,n}$ by the coefficients and functions corresponding to the IG modes. In Fig. 3(a) we depict efficiency values $\eta_{4,n}$, for several orders n, which correspond to the KPE of the HG beam $f_{4,4}$. As expected, the highest efficiency value is $\eta_{4,4}$. In Fig. 3(b) we depict efficiency values $\eta^{o}_{m,5}$, for several orders m, which correspond to the KPE $k^{o}_{9,5}$. In this case, the highest efficiency value is $\eta^{o}_{9,5}$. In the considered cases, the efficiency for the encoded mode is at least two orders of magnitude larger than the efficiencies for the remaining modes.

In Tables 3 and 4 we show the efficiencies $\eta_{m,n}$ and $\eta^{\alpha}_{m,n}$, corresponding to the encoded modes, for several KPEs $k_{m,n}$ and $k^{\alpha}_{m,n}$. It is found that such efficiencies tend to reduce when any of the indices increases (maintaining the other index fixed). This tendency indicates that the dominance of the encoded mode for each KPE reduces with the increment of the indices. Since the reduction in the dominance of the encoded mode, which corresponds to a lower weighting factor, makes this mode more sensible to the noise originated in the remaining modes, this result also explains the increment of the RMS (Tables 1 and 2) when the indices increase.

4. EXPERIMENTAL GENERATION OF THE BEAMS

The experimental setup we employed to generate Hermite–Gauss and Ince–Gauss beams is depicted in Fig. 4. An expanded and collimated He–Ne laser beam (LB) is employed

Table 2. RMS for (a) Even and (b) Odd IG Beams Generated with Their KPEs

(a)

				n			
m	**0**	**1**	**2**	**3**	**4**	**5**	**6**
0	0.0136						
1		0.0198					
2	0.0323		0.0320				
3		0.0458		0.0408			
4	0.0629		0.0403		0.0428		
5		0.0672		0.0413		0.0510	
6	0.0783		0.0345		0.0351		0.0546

(b)

				n			
m		**1**	**2**	**3**	**4**	**5**	**6**
1		0.0199					
2			0.0314				
3		0.0433		0.0366			
4			0.0747		0.0446		
5		0.0805		0.0615		0.0459	
6			0.0935		0.0525		0.0497

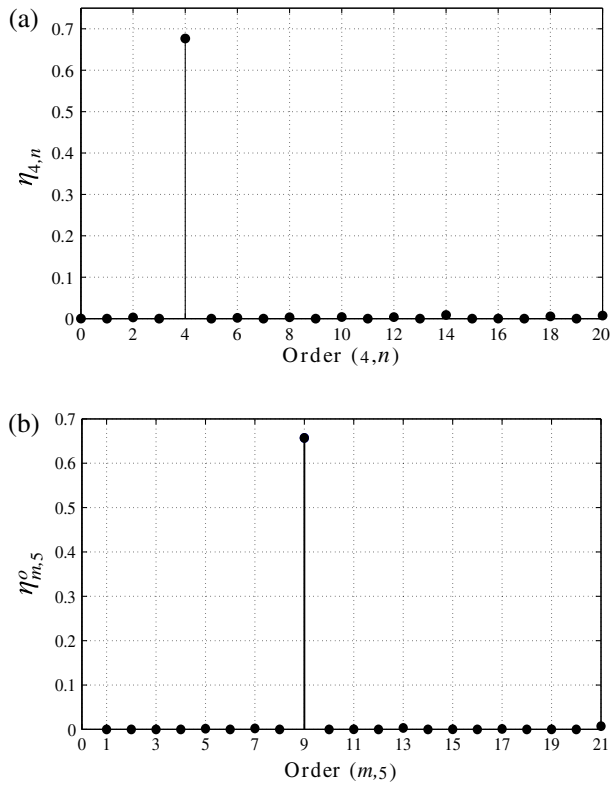

Fig. 3. Efficiencies (a) $\eta_{4,n}$ and (b) $\eta^o_{m,5}$ in the generation of different modes ($f_{4,n}$ and $f^o_{m,5}$) through the KPEs $k_{4,4}$ and $k^o_{9,5}$, respectively.

to illuminate a circular pupil (P). A double Fourier transform array, formed by a couple of lenses (L_1, L_2) of equal focal lengths f, projects an image of the pupil into the plane of a phase spatial light modulator (SLM). We avoid the use of a single-lens image projector that would introduce a quadratic phase modulation. This projected image pupil is intended to cover the aperture of the displayed KPE. The SLM is aligned to reflect the incoming light in a new axis that forms an angle θ with the incoming axis. The employed phase SLM is a reflective device (HOLOEYE Photonics AG), with a transverse resolution of 8 μm and a dynamical range of 2π radians. The KPEs, which are encoded in the SLM, are Fourier transformed by lens L_3. The intensities of such Fourier spectra are recorded by a CCD. In order to avoid unmodulated reflected light in the KPE Fourier domain, its transmittance is multiplied by two different blazed gratings, one inside the pupil area and the other in the remaining area.

In Figs. 5(a)–5(d) we show the numerically generated intensities of the Fourier transform of $f_{4,4}$, $k_{4,4}$, $f^e_{6,6}$, and $k^e_{6,6}$, respectively. The computed phases of these fields and corresponding KPEs are depicted in Figs. 5(e)–5(h). The phase in Fig. 5(h) presents incorrect variations at the edge of the circular domain. However, such errors are not very significant since they appear at sections of the field [see Fig. 5(d)] with low amplitude.

We implemented experimentally KPEs for HG and IG beams with different indices (m, n). Figures 6, 7, and 8 show results that correspond to the cases of HG, even IG, and odd IG beams, respectively. Each one of these figures includes theoretical beam intensities that correspond to the images in the first column. The intensities of beams generated by the KPEs are displayed in the second column (numerical simulations) and third column (experimental results). We point out that the considered fields are expressed by real type functions. Therefore, the phases of these fields have only two values: 0 for the positive sections of the fields and π for the negative parts. Such binary phases have been illustrated in Figs. 1 and 5. The KPEs for HG beams corresponds to indices ($m = 4$, n) for $n = 0, 1, \ldots 4$. The beam waist in this case was $w_o = 512$ μm. In the cases corresponding to IG beams, the employed beam waist is $w_o = 256$ μm, and the beam indices adopt a variety of values that are shown in Figs. 7 and 8.

Results in Figs. 6, 7, and 8 show that the intensities of beams generated by KPEs present marginal errors with respect to the theoretical results [column (a) in each case]. Such errors have been evaluated by the RMS values computed in Section 3. In all cases, experimental [column (c)] and numerical [column (b)] results are quite similar.

5. DISCUSSION AND FINAL REMARKS

Now we briefly discuss why the desired field is visible in the Fourier domain of the KPEs. It was proved in Section 2 that the KPEs of the desired HG or IG modes are the phase DOEs whose orthogonal series contain these fields with the maximum possible weighting factor. In Sections 3 and 4 we have demonstrated, by means of numerical simulations and experimentally, that approximate versions of the HG and IG beams can be generated at the Fourier domain of their KPEs. To understand this result, we will focus our attention to the case of a HG beam. Nevertheless, the arguments employed in this case can be extended to the case of IG beams.

First of all, we note that the orthogonal series in Eq. (3), for the KPE transmittance, can be expressed as

Table 3. Efficiencies $\eta_{m,n}$ in the Generation of Modes $f_{m,n}$ Employing the KPEs $k_{m,n}$ for Different Indices (n, m)

	n						
m	0	1	2	3	4	5	6
0	0.7751	0.7521	0.7369	0.7321	0.7243	0.7222	0.7167
1		0.7297	0.7150	0.7104	0.7027	0.7007	0.6953
2			0.7005	0.6960	0.6885	0.6866	0.6813
3				0.6915	0.6841	0.6822	0.6769
4					0.6767	0.6748	0.6696
5						0.6729	0.6677
6							0.6626

Table 4. Efficiencies $\eta^{\alpha}_{m,n}$ for Different Allowed Orders of (a) Even and (b) Odd IG Beams Generated Through the KPE $k^{\alpha}_{m,n}$

(a)

	n						
m	0	1	2	3	4	5	6
0	0.7927						
1		0.7388					
2	0.7016		0.7259				
3		0.7181		0.7034			
4	0.6158		0.7061		0.6857		
5		0.6595		0.6665		0.6605	
6	0.5579		0.7049		0.6640		0.6391

(b)

	n						
m		1	2	3	4	5	6
1		0.7463					
2			0.6973				
3		0.6644		0.6879			
4			0.6544		0.6768		
5		0.5848		0.6648		0.6602	
6			0.6144		0.6649		0.6418

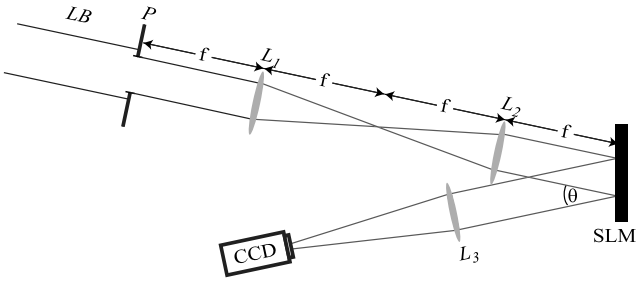

Fig. 4. Experimental setup to generate HG and IG beams. The KPE is codified on the SLM and a CCD camera is placed at the Fourier plane of lens L_3.

$$k_{m,n}(x,y;w_o) = A_{m,n} f_{m,n}(x,y;w_o) + d_{m,n}(x,y;w_o), \quad \textbf{(17)}$$

$$d_{m,n}(x,y;w_o) = \sum_{(p,q)\neq(m,n)}^{\infty} A_{p,q} f_{p,q}(x,y;w_o). \quad \textbf{(18)}$$

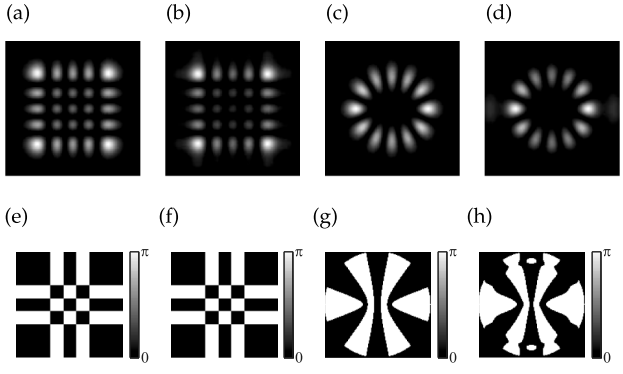

Fig. 5. Intensities of the Fourier spectra (a) $F_{4,4}$, (b) $K_{4,4}$, (c) $F^{e}_{6,6}$, and (d) $K^{e}_{6,6}$. The corresponding phases are displayed, respectively, in the bottom images [(e), (f), (g), and (h)].

In Eq. (17), the KPE transmittance is formed by the desired term (with coefficient $A_{m,n}$) and the "difference" term $d_{m,n}(x,y;w_o)$, which according to Eq. (18) contains all the HG modes with combined indices different than (m,n), which are orthogonal to $f_{m,n}(x,y;w_o)$. As proved in Section 2, the first term in Eq. (17) is dominant. However, such a term that corresponds to the desired field is not visible at the KPE plane, whose intensity is uniform within its limiting pupil.

An interesting result is that the Fourier transform of the HG beam [Eq. (1)] is given, omitting a constant factor, by $(-i)^{p+q} f_{p,q}(u,v;w_o')$ [11], where (u,v) are frequency coordinates in the Fourier domain and $w_o' = (\pi w_o)^{-1}$. Considering this result, the Fourier transform of the KPE is expressed as

$$K_{m,n}(u,v;w_o) = (-i)^{m+n} A_{m,n} f_{m,n}(u,v;w_o') + D(u,v;w_o'), \quad \textbf{(19a)}$$

$$D(u,v;w_o') = \sum_{(p,q)\neq(m,n)}^{\infty} (-i)^{p+q} A_{p,q} f_{p,q}(u,v;w_o'). \quad \textbf{(19b)}$$

It is noteworthy in Eq. (19) that the Fourier transform of the kinoform is a series of orthogonal HG modes, similar to that in Eq. (3), except for the phase factor $(-i)^{p+q}$ that modulates the (p,q)-order mode. In Eq. (19a), the (m,n)-term is still dominant with respect to the other terms that appear in the function $D(u,v;w_o')$. However, the HG modes in $D(u,v;w_o')$, which are modulated by the discrete phase factor $(-i)^{p+q}$ and periodic in the power $p+q$, are now superposed in a destructive form, opening the possibility of making visible the dominant term.

As an additional argument to understand how the desired HG beam can be generated employing its KPE, we note that the KPE transmittance [Eq. (2)] presents acute dislocations at each position where the sign of $f_{m,n}(x,y;w_o)$ is inverted and at the edges of the limiting pupil $\mathrm{rect}(x/a, y/b)$, where the KPE abruptly becomes null. On the other hand, we note that the first right-side term in Eq. (17) is a continuous and derivable

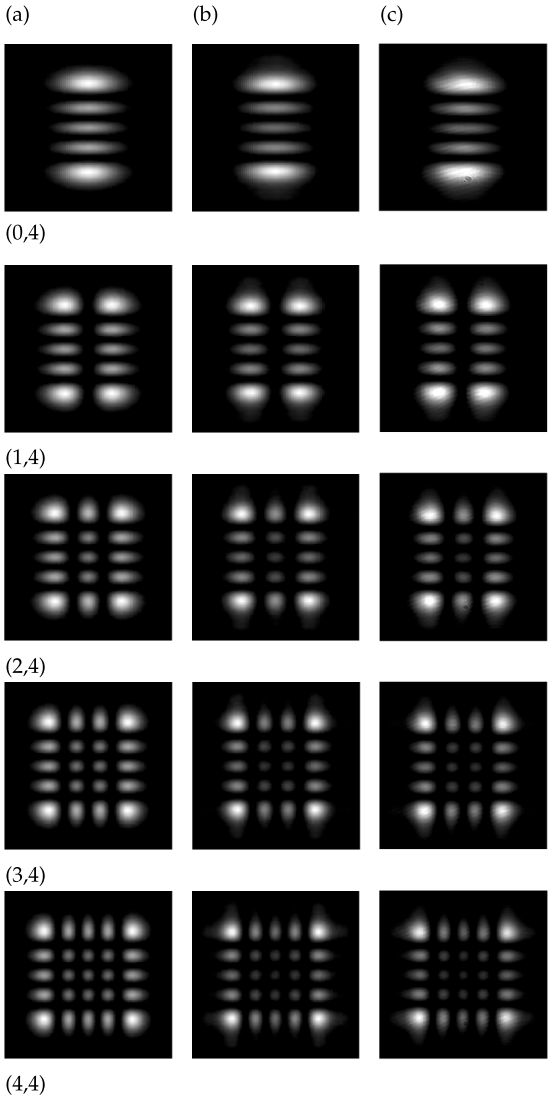

Fig. 6. Column (a) shows the intensities of HG beams Fourier spectra $F_{n,m}$ for several indices (n, m). The intensities of the Fourier spectra of the corresponding KPEs are displayed in column (b) numerical and column (c) experimental.

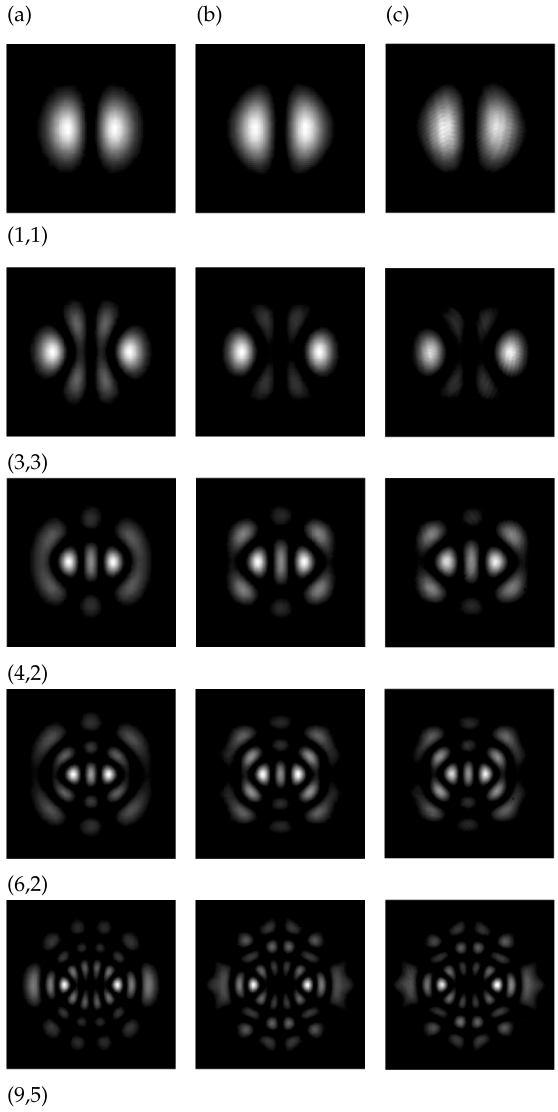

Fig. 7. Theoretical intensities of IG beams Fourier spectra $F^{e}_{n,m}$ for several indices (n, m) are shown in column (a). Numerical and experimental intensities of the Fourier spectra of the corresponding KPEs are displayed in column (b) and column (c), respectively.

function. Therefore, each one of the KPE dislocations must correspond to a dislocation in the field $d_{m,n}(x, y; w_o)$. Because of such dislocations, it is expected that the Fourier spectrum of $d_{m,n}(x, y; w_o)$ will appear distributed in a domain much larger than the domain of $F_{m,n}(u, v; w_o)$, which makes this field visible in the KPE Fourier domain.

To illustrate the preceding assertions, let us consider that the desired HG beam is $f_{2,2}(x, y; w_o)$. The horizontal transverse profile for the KPE of this beam, with an optimized pupil, is shown (solid trace) in Fig. 9(a). Such a transverse profile is taken along an axis that includes the beam peak intensity. The transverse profiles of the computed fields $A_{2,2} f_{2,2}(x, y; w_o)$ (dashed trace) and $d_{2,2}(x, y; w_o)$ (dotted trace) are also displayed in Fig. 9(a). As expected, each dislocation in the KPE corresponds to a dislocation in $d_{2,2}(x, y; w_o)$. On the other hand, in Fig. 9(b) we show the horizontal transverse profiles of the KPE Fourier spectrum (for this example) and for their two components, which appear at the right side of Eq. (19a). These transverse profiles are also chosen in order to include the peak amplitude of the KPE Fourier spectrum. It is noted that the KPE Fourier spectrum (solid trace) is quite similar to the spectrum of the desired mode (dashed trace), within the field domain. In addition, it is noteworthy that the Fourier spectrum of the difference term (dotted trace) is extended in a domain which is relatively larger than the domain of the desired field. Far from the origin, where the desired mode field is approximately zero, the KPE and difference fields are coincident. In Fig. 10 we show similar results at the Fourier domain of KPEs for the HG modes $f_{3,3}(x, y; w_o)$ and $f_{4,4}(x, y; w_o)$.

The generation of HG and IG beams can be performed by means of resonant cavities [12,13] and by the use of synthetic phase holograms that have the capability of generating arbitrary

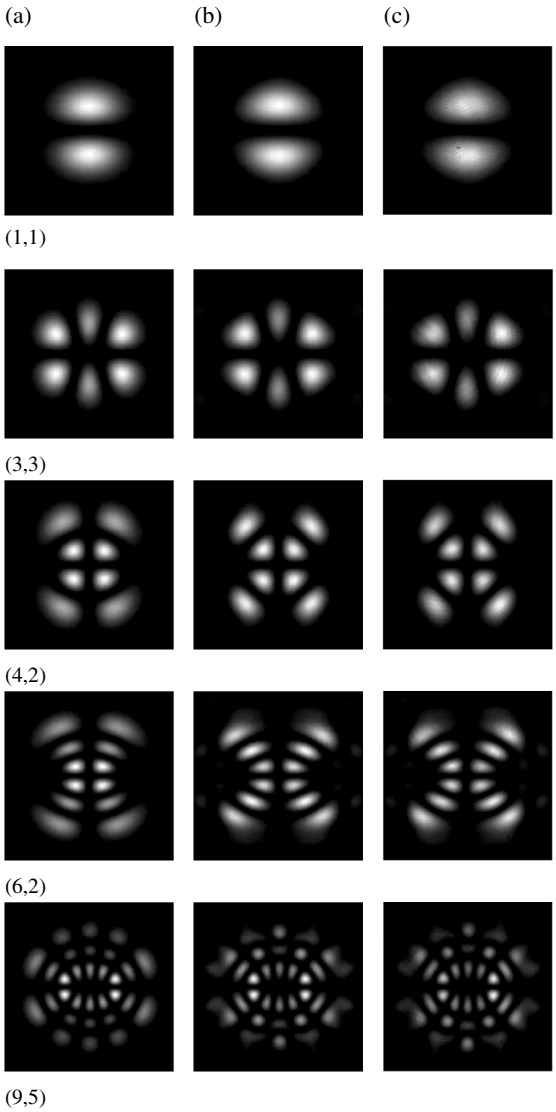

Fig. 8. Results similar to those in Fig. 7, corresponding to odd IG beams and associated KPEs.

complex fields [8,14,15]. The analysis and comparison of these techniques with our simple method presented here are beyond the scope of the present report.

Summarizing, we have discussed the optical generation of Hermite–Gauss and Ince–Gauss beams employing KPEs. It is noteworthy that approximated versions of the desired beams appear at the Fourier domain of the KPEs. When an appropriate pupil size is employed, the method synthesizes HG and IG beams with relatively high accuracy and high efficiency. Indeed, it has been proved that, in the context of the employed approach, the KPEs are the phase elements that generate the desired beams with the maximum possible efficiency. For the discussed KPEs, intended to generate a variety of HG and IG beams, the computed efficiencies are in the range of 0.55 and 0.79, whereas the RMS values are in the range of 0.013 and 0.094. A comparison of the experimental and numerical results with the theory shows a remarkable agreement.

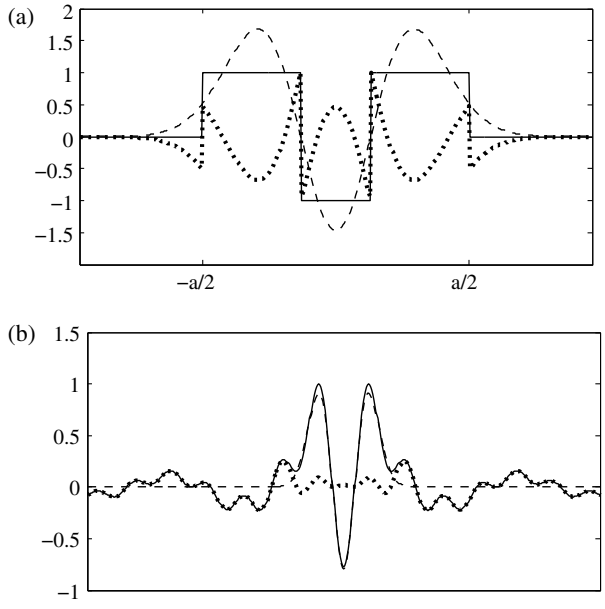

Fig. 9. (a) Cross section of the KPE for the HG beam $f_{2,2}$ (solid line), together with the dominant mode $A_{2,2}f_{2,2}$ (dashed line) and the difference term $d_{2,2}$ (dotted line), in the KPE orthogonal series. (b) Cross section of the KPE Fourier transform $F_{2,2}$ (solid line), together with the Fourier spectra of the dominant mode (dashed line), and the difference term (dotted line).

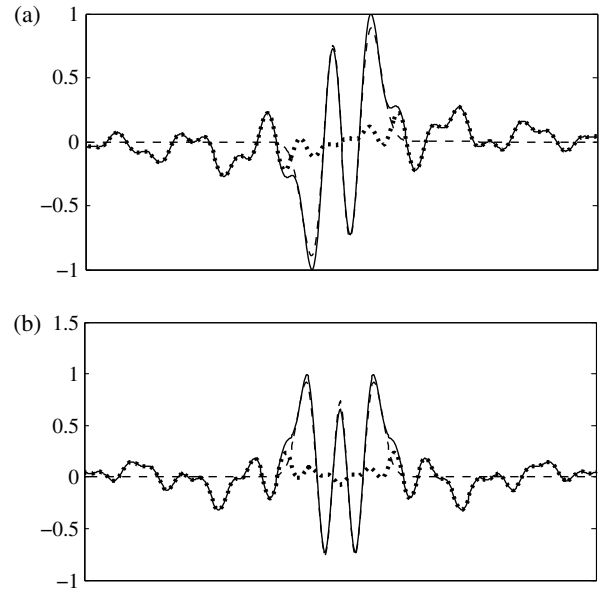

Fig. 10. Similar results to that in Fig. 9(b), for KPEs of the HG beams (a) $f_{3,3}$ and (b) $f_{4,4}$.

Funding. CONACYT (322012, 367016).

REFERENCES

1. J. T. Verdeyen, *Laser Electronics* (Prentice-Hall, 1995).
2. M. A. Bandres and J. C. Gutiérrez-Vega, "Ince–Gaussian modes of the paraxial wave equation and stable resonators," J. Opt. Soc. Am. A **21**, 873–880 (2004).

3. V. Arrizón, D. Sánchez-de-la-Llave, U. Ruiz, and G. Méndez, "Efficient generation of an arbitrary nondiffracting Bessel beam employing its phase modulation," Opt. Lett. **34**, 1456–1458 (2009).
4. V. Arrizón, D. Sánchez-de-la-Llave, G. Méndez, and U. Ruiz, "Efficient generation of periodic and quasi-periodic non-diffractive optical fields with phase holograms," Opt. Express **19**, 10553–10562 (2011).
5. V. Arrizón, U. Ruiz, D. Aguirre-Olivas, D. Sánchez-de-la-Llave, and A. S. Ostrovsky, "Comparing efficiency and accuracy of the kinoform and the helical axicon as Bessel–Gauss beam generators," J. Opt. Soc. Am. A **31**, 487–492 (2014).
6. R. J. Hernández-Hernández, R. A. Terborg, I. Ricardez-Vargas, and K. Volke-Sepúlveda, "Experimental generation of Mathieu–Gauss beams with a phase-only spatial light modulator," Appl. Opt. **49**, 6903–6909 (2010).
7. N. Matsumoto, T. Ando, T. Inoue, Y. Ohtake, N. Fukuchi, and T. Hara, "Generation of high-quality higher-order Laguerre–Gaussian beams using liquid-crystal-on-silicon spatial light modulators," J. Opt. Soc. Am. A **25**, 1642–1651 (2008).
8. J. B. Bentley, J. A. Davis, M. A. Bandres, and J. C. Gutiérrez-Vega, "Generation of helical Ince–Gaussian beams with a liquid-crystal display," Opt. Lett. **31**, 649–651 (2006).
9. V. Arrizón, D. Sánchez-de-la-Llave, and G. Méndez, "Holographic generation of a class of nondiffracting fields with optimum efficiency," Opt. Lett. **37**, 2154–2156 (2012).
10. M. A. Bandres and J. C. Gutiérrez-Vega, "Ince–Gaussian series representation of the two-dimensional fractional Fourier transform," Opt. Lett. **30**, 540–542 (2005).
11. D. Mendlovic and H. M. Ozaktas, "Fractional Fourier transforms and their optical implementation: I," Opt. Lett. **10**, 1875–1881 (1993).
12. H. Kogelnik and T. Li, "Laser beams and resonators," Appl. Opt. **5**, 1550–1567 (1966).
13. U. T. Schwarz, M. A. Bandres, and J. C. Gutiérrez-Vega, "Observation of Ince–Gaussian modes in stable resonators," Opt. Lett. **29**, 1870–1872 (2004).
14. V. Arrizón, G. Méndez, and D. Sánchez-de-La-Llave, "Accurate encoding of arbitrary complex fields with amplitude-only liquid crystal spatial light modulators," Opt. Express **13**, 7913–7927 (2005).
15. V. Arrizón, U. Ruiz, R. Carrada, and L. A. González, "Pixelated phase computer holograms for the accurate encoding of scalar complex fields," J. Opt. Soc. Am. A **24**, 3500–3507 (2007).